Natural Resources Research, Vol. 30, No. 1, February 2021 (© 2020)
https://doi.org/10.1007/s11053-020-09707-2

Original Paper

Size Reduction Characterization of Underground Mine Tailings: A Case Study on Sandstones

Ekin Köken[1,2]

Received 2 April 2020; accepted 20 May 2020
Published online: 9 June 2020

The production of construction and building materials starts with reducing the size of natural, industrial, and waste materials. In addition to strength and durability considerations of natural resources recommended by various institutions, size reduction characterization, specific to rock aggregates, has a vital role in their size-related quality. In this study, various sandstones extracted from underground mines located in northwestern Turkey were investigated for size reduction characterizations. Several mineralogical, textural, and physico-mechanical properties were determined for each rock type. Crushability tests were carried out using a laboratory-scale cone crusher for different feeding size fractions, namely + 11.20 − 16.00 mm (size I), + 9.52 − 16.00 mm (size II), and + 6.30 − 16.00 mm (size III). Based on the crushability tests, crushed particles were analyzed, focusing on production yield, size, and shape properties. Each crushability test was also explored for energy consumption arising from varying rock properties of the sandstones. The laboratory test results demonstrated that the degree of rock crushability (DRC) and specific energy consumption (E_{cs}, kJ/kg) were associated with the Brazilian tensile strength (BTS, MPa) and apparent porosity (n_e, %) of the sandstones. The results also showed that the degree of sorting in mineral constituents, quantified as the sorting coefficient (S_c), affected the DRC. However, mineralogical features of the sandstones have no significant impact on DRC and E_{cs}. Variations in feeding gradation, irrespective of whether mineralogical, textural, or physico-mechanical properties, have remarkable effects on product flakiness and yields for specific size fractions. In light of the findings obtained, the present study provides knowledge on how the sandstones behave under cone crushing operations.

KEY WORDS: Sandstone, Mine tailing, Size reduction, Cone crusher, Rock aggregate.

INTRODUCTION

Size reduction characterization and assessment of natural resources, industrial materials, and their tailings are important considerations in projects related to production engineering, rock aggregate science and technology, mineral processing, and the development of new techniques about waste management systems. The size reduction process, in this regard, is a part of geometallurgy that comprises various interrelated disciplines such as mineralogy, petrography, geostatistics, metallurgy, and material sciences. Specific to natural resources, the rock comminution starts with crushing rocks through various crushers. An economical, productive, and sustainable rock quarrying should meet certain requirements, namely obtaining products cubical and angular in shape, optimization of specific energy consumption, and satisfying desired product capac-

[1]Department of Materials Science and Nanotechnology Engineering, Abdullah Gül University, 38100 Kayseri, Turkey.
[2]To whom correspondence should be addressed; e-mail: ekin.koken@agu.edu.tr

ity with less amount of fine and flaky products (Briggs and Evertsson 1998; Major 2002; Mitchell et al. 2008; Major 2009; Wills and Finch 2015; Lynch 2015; Gupta and Yan 2016). Based on rock aggregate manufacturing, crushing operations may be divided into three main phases, such as primary, secondary, and tertiary crushing operations, each of which has several specifications regarding the use of different belt conveyor systems, screens, and types of crushers (Leiva et al. 2018).

On the one hand, the size of enormous rock blocks obtained from drilling to blasting operations is reduced at primary crushing operations, where jaw, gyratory, and horizontal shaft impact (HSI) crushers are mainly used. On the other hand, cone, HSI, and vertical shaft impact (VSI) crushers are preferred for secondary and tertiary crushing processes (Fig. 1). According to Metso (2018), a Finnish industrial machinery company providing technology and service for rock aggregate science and technology, the economic value of rock aggregates is not only dependent upon strength properties but also on its size fractions (Fig. 1). It has been experienced that the quality and performance of engineering structures associated with rock aggregates have a direct relationship with the quality, size, and shape properties of rock aggregates. For instance, the water/cement ratio for concrete structures is adjusted, considering the variations in the rock aggregate size being used. Therefore, an optimal rock aggregate gradation provides a higher packing degree that increases the strength of concrete structures (Smith and Collis 2001). More specifically, rock aggregates below 25 mm have been of outstanding importance in investigating the compaction degree of pavements, the durability of concretes, and the design of asphalt mixtures (Kozul and Darwin 1997; Coree and Hislop 2000; Akçaoğlu et al. 2004; Chen et al. 2005; Chen and Liu 2007; Elices and Rocco 2008; Vu et al. 2011; Golalipour et al. 2012; Kuity and Das 2016; Kim et al. 2018; Sadrmomtazi et al. 2020; Khasawneh and Alsheyab 2020). Concerning railway infrastructures, rock aggregates with particle sizes ranging from 31.5 to 63 mm have been identified as railway ballast whose quality, size, and shape properties have been specified elaborately (BS EN 13450 2002).

Regarding the previously mentioned studies, industrial size-related rock aggregate manufacturing deals mainly with secondary and tertiary crushing operations (Fig. 1). Over the past three decades, the factors affecting the degree of rock crushability (DRC) and rock–crusher interrelations have been investigated profoundly from many aspects. Primarily, lithological variances in rocks have substantial impacts on both their attrition typology and behavior under compressive loading. Furthermore, the closed side setting (CSS), stroke, and eccentric speed (E_s) are the essential characteristics of compressive crushers that affect the DRC (Heikkilä 1991). Eloranta (1995) showed that the particle size distribution (PSD) of feeding material and the CSS of cone crushers play a significant role in the product flakiness.

Bearman et al. (1997) concluded that the tensile strength of rocks has a remarkable effect on the performance of cone crushers. Donovan (2003) found that fracture toughness, as a mechanical rock property, has a close link to crushing energy consumption in jaw crushers. Djordjevic et al. (2003) performed simulations for the assessment of rock fragmentation in VSI and HSI-type crushers by using the discrete element method (DEM). Researchers have pointed out that the DEM can be utilized in several issues related to modeling the particle flow behavior, energy utilization, and product size estimations of the crushers considered. Nikolov (2004) introduced a dynamic particle model indicating that the impact of energy per unit mass in VSI crushers is higher than that of HSI crushers. Guimaraes et al. (2007) found that intensive particle–particle interaction takes place during crushing operations when the choke feeding method is adopted. Furthermore, researchers also concluded that the generation of fines increases with increasing shear forces during rock aggregate production.

Lee and Evertsson (2011) stated that the setup of the cone crushing process affects the PSD of the product such that increasing the CSS of the cone crusher leads to size reduction. Moreover, an adjustment in broader strokes in cone crusher relatively increases the production yield for specific size fractions. Numbi et al. (2014) presented a control model feasible to improve the crushing process of VSI-type crushers. Bengtsson et al. (2015) expressed the complexities of crushing plants that could be handled by employing simulations. Notably, the researchers carried out successful simulations to estimate product flakiness and capacities. Ma et al. (2016) showed that the variations in the PSD of feeding material have influences on the wear rate of the cone crusher.

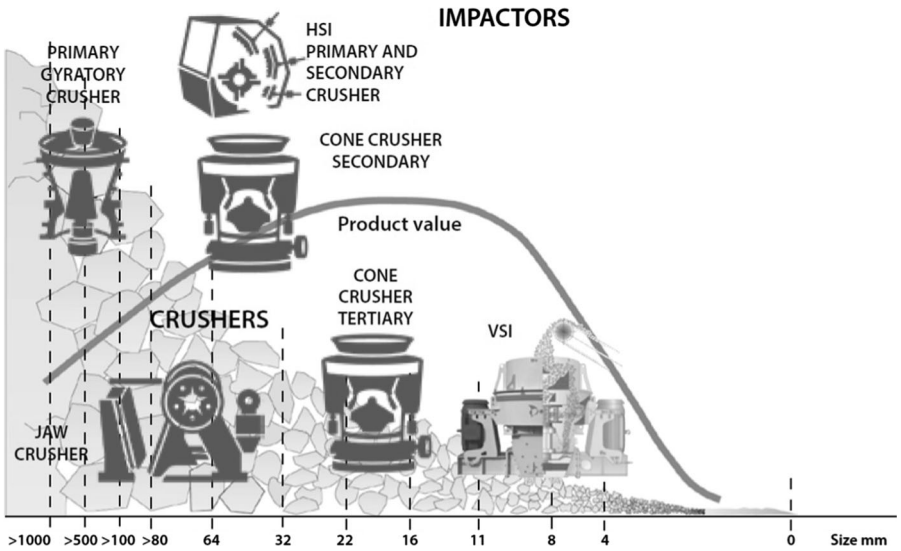

Figure 1. Crusher types used in rock aggregate manufacturing (Metso 2018).

The researchers also indicated that increasing the particle size of the feeding material causes a higher degree of wear in cone crusher liners.

Korman et al. (2015) performed extensive research for the assessment of crushing energy consumption occurring in a laboratory-scale jaw crusher. Their laboratory test results indicated that the uniaxial compressive strength (UCS, MPa) of rocks affects the crushing energy consumption. Similarly, Köken and Özarslan (2018) introduced a testing methodology, compressive crushing value (CCV), for evaluating the DRC in jaw crushers. It was shown that the DRC can be quantified by variations in the CCV, where lower CCVs indicate higher crushing resistance of rocks. Moreover, it was also determined that the CCV is highly dependent on the UCS of rocks. Ulsen et al. (2019) considered recycled concrete aggregates to investigate relationships between their secondary crushability by the jaw and impact crushers and their fundamental aggregate properties (e.g., water absorption, porosity, and degree of binding). It was concluded that there are no significant differences in the aggregate properties arising from the crusher type. Recently, Bhaadani et al. (2020) introduced several performance factors to improve rock aggregate production in crushing–screening plants. Based on this study, rock aggregate production processes were monitored with the help of performance maps indicating the variations in the capacity, PSD, and product flakiness as well.

Moreover, this study has highlighted the importance of the calibration and/or adjustment of operational factors (e.g., the CSS, throw, and orientation of screens) for achieving a more functional rock crushability. Just as importantly, Rajan and Singh (2020) investigated the variations in rock aggregate morphology produced from various crusher circuits. It was concluded that the rock aggregate angularity is associated with the order of crushers, where the rocks are charged. The aforementioned studies have come up with sound fundamentals of rock crushability, significant factors related to rock aggregate production through various crushers, and reasonable solutions/methods for handling an optimum rock quarrying.

The present study aimed to explore the DRC of sandstones located in northwestern Turkey. The study encompassed mineralogical, textural, and physico-mechanical measurements for characterizing the sandstones. The DRC of sandstones was investigated, using a laboratory-scale cone crusher. For the quantification of the DRC, crushability tests were performed using sandstone aggregates with different size fractions. The results were then compared with the mineralogical, textural, and physico-mechanical properties of rocks. As a result of the laboratory studies, size reduction characterization of the sandstones was revealed, considering a compre-

hensive approach that includes production yield, size, and shape properties of the crushed particles obtained from the crushability tests.

MATERIALS AND METHODS

Study Area and Materials Studied

Representative sandstone blocks were obtained from ten different underground mines located in Northwestern Turkey. As for the study area, Northwestern Turkey, from Zonguldak to Kastamonu (Fig. 2), is the only region endowed with a vast amount of hard coal deposits in the country. This region is referred to as Zonguldak Hardcoal Basin (ZHB). Due to intensive underground mining applications in the ZHB, coal measure rocks, especially sandstones, have been extracted regularly. In general, the sandstones extracted from underground mining applications in the ZHB have been regarded neither as a rock aggregate source nor an industrial material. Despite their increasing tonnage, these sandstones have been acknowledged as a kind of mine tailing. The presence of these rocks, together with their derivatives, poses seemingly a problem in terms of environmental issues and waste management in the ZHB. Thus, various sandstones (Sk–1; Sag–10) in the ZHB were considered in terms of size reduction characterization as a starting point for investigating their potential use in various areas.

Methods

Before performing crushability tests, mineralogical, textural, and physico-mechanical properties were defined for each rock type. The physical and mechanical properties were determined for each rock type, following the methods suggested by the International Society for Rock Mechanics (ISRM 2007). The mineralogical and textural characterizations of the sandstones were also performed by thin-section analyses. Based on the crushability tests, production yield was investigated by detailed sieve analyses for each rock type. Furthermore, the variations in the shape of the crushed particles were investigated through flakiness index tests and image analyses. The crushing patterns of the sandstones were also investigated by scanning electron microscope (SEM) analyses, where a Gemini SEM 300 analyzer was used.

The flakiness index tests were performed following BS EN 933–3 (2012). Image analyses were carried out using high–resolution images (1920 × 1080 pixels) of the crushed particles with different size fractions such as − 9.52 mm + 6.30 mm, − 6.30 + 4.75 mm, and − 4.75 mm + 2.36 mm. A typical illustration of image analyses is shown in Figure 3.

During thin-section analyses, the mineral grain, whose elongation ratio (ER) was greater than 2, was declared flaky. The ER was thereby a function of maximum and minimum Feret diameters (F_{max}, F_{min}) of crushed particles and determined by the following equation:

$$\mathrm{ER} = F_{max}/F_{min} \tag{1}$$

where F_{max} and F_{min} are maximum and minimum Feret diameters (mm) of crushed particles, respectively.

In the context of the mineralogical and textural analyses, the quantity of rock-forming minerals (i.e., quartz (Qtz), feldspar (F), lithic fragment (Lf)), average grain size (d_{50}, mm), and sorting coefficient (S_c) was determined. In thin-section analyses, the point counting method described by Dickinson (1970) was adopted to quantify rock-forming minerals. The determinations of the d_{50} and S_c deal with calculating surface areas (A_c) of rock-forming minerals and analyzing them for specific areas occupied in thin sections. The A_c of rock-forming minerals was digitized using MATLAB R2019a and was determined as:

$$A_c = \frac{1}{2}\left|\sum_{i=1}^{n} x_i(y_{i+1}) - \sum_{i=1}^{n} y_i(x_{i+1})\right| \tag{2}$$

where x_i and y_i are digitized coordinates of the grain boundary surfaces.

For specific areas (e.g., 20–50 mm^2) in each thin section, surface areas of rock-forming minerals were determined and analyzed statistically. Because anhedral, euhedral, and subhedral mineral constituents can be assumed as somewhat spherical, elliptical, and prismatic in such cases, the A_c of rock-forming minerals is determined by Eq. (2).

The quantification of equivalent diameter (D_e) of any mineral grain is related to A_c and Feret diameters of the grain. Consequently, D_e is a function of these variables and it was determined by the following equation, which is a modification from the study of Huebscher (1948):

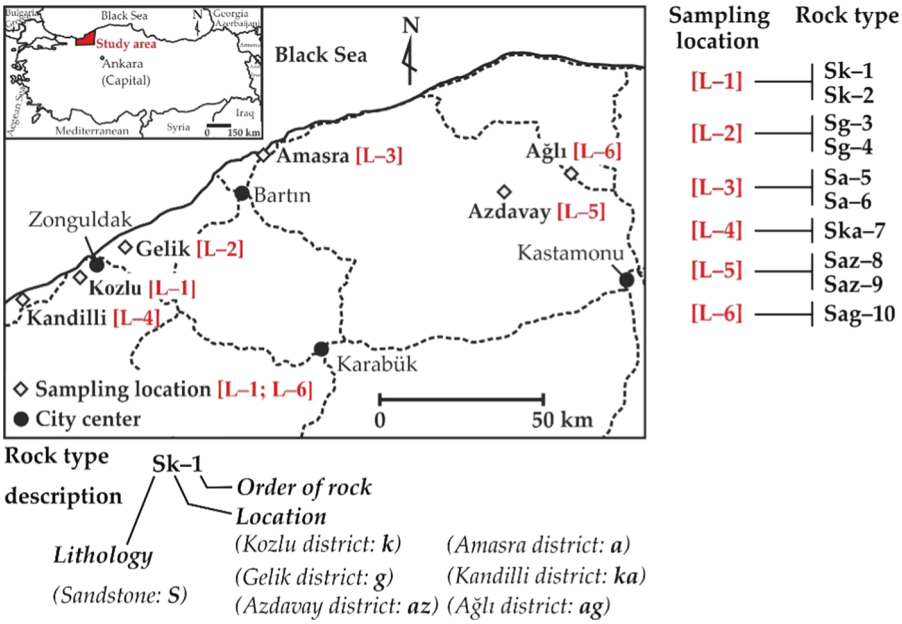

Figure 2. Sampling location map of the study area.

$$D_e = 0.56(A_c)^{0.500} + 0.65\left(\frac{(F_{max}F_{min})^{0.625}}{(F_{max}+F_{min})^{0.250}}\right) \quad (3)$$

Based on D_e values, the S_c was determined using the following equations:

$$\phi = -\log_2(D_e) \quad (4)$$

where ϕ is the size value of the grain and D_e is in mm,

$$S_c = \frac{\phi_{84} - \phi_{16}}{4.0} + \frac{\phi_{95} - \phi_5}{6.6} \quad (5)$$

where ϕ_{95}, ϕ_{84}, ϕ_{16}, and ϕ_5 represent the statistical size values corresponding to 95%, 84%, 16%, and 5% of the cumulative density function of the analyzed grains, respectively (Folk and Ward 1957). The determinations of the d_{50} and S_c are illustrated in Figure 4.

Based on several image analysis techniques (i.e., scaling, separation, and filtering), the boundaries of rock-forming minerals were digitized using MATLAB 2019a. For each rock type, five representative thin sections were analyzed, and the average values obtained from Eqs. (3) and (5) were presented as d_{50} and S_c, respectively. After the determinations of mineralogical, textural, and physico-mechanical properties, the size reduction characterization of the sandstones was investigated using a laboratory-scale cone crusher, whose technical properties are listed in Table 1. The experimental flowchart for the crushability tests is shown in Figure 5. Three different size fractions (sizes I–III) were considered in the crushability tests.

For each crushability test, the CSS of the crusher was set to 8 mm. The E_s and the stroke of the cone mantle were 690–700 rpm and 10 mm, respectively. The total energy (E_T, kJ) consumed during the crushability test was calculated as:

$$E_T = \frac{V_n \times I_{d-ave} \times T_c}{10^3} \quad (6)$$

where V_n is the nominal voltage (V), $I_{d\text{-}ave}$ is the average current drawn by the crusher during crushing action (A), and T_c is the elapsed time (s) throughout the crushing operation.

Considering E_T, the specific energy consumption (E_{cs}, kJ/kg) was determined as:

$$E_{cs} = \frac{E_T}{10^{-3} \times m_f} \quad (7)$$

where m_f is the total mass (g) of feeding material.

Because the amount of energy applied to rock materials determines the DRC (Itävuo et al. 2013), the variations in energy consumption arising from mineralogical and textural variances of the sand-

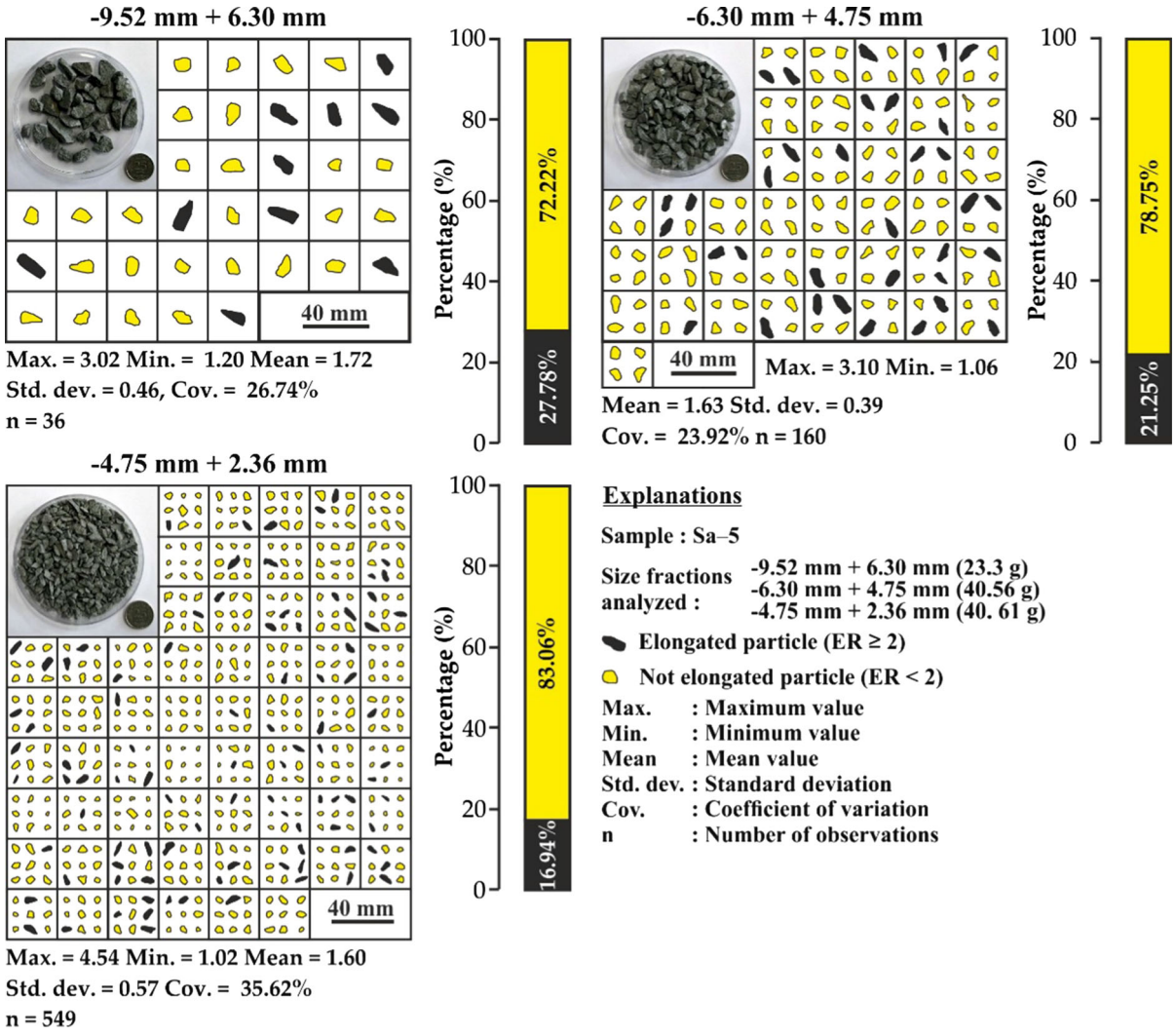

Figure 3. Illustration of image analyses for the determination of product flakiness.

stones were also investigated. The DRC of sandstones was determined, considering two simple approaches, one of which was the Taggart method.

In practical approaches to minerals engineering, the performance of crushers and mills has been investigated by the Taggart method (Metso 2018), whereby the size reduction ratio (SRR) is determined as:

$$\mathrm{SRR} = \frac{F_{80}}{P_{80}} \tag{8}$$

where F_{80} and P_{80} are the theoretical square mesh aperture sizes (mm) corresponding to 80% of cumulative undersize of feed's and product's PSDs, respectively.

The other method for assessing the DRC is the size distribution width (Δ_n) proposed by Evertsson (1999). Variations in Δ_n provide knowledge about the production yield profile of related crushing operation for specific size fractions. The Δ_n is determined as:

$$\Delta_n = \frac{P_{80} - P_{20}}{P_{50}} \tag{9}$$

where P_{80}, P_{50}, and P_{20} are the theoretical square mesh aperture sizes (mm) that correspond to 80%, 50%, and 20% of cumulative undersize of product's PSDs, respectively.

In flakiness index tests, various bar sieves were used for different size fractions of the feed and product.

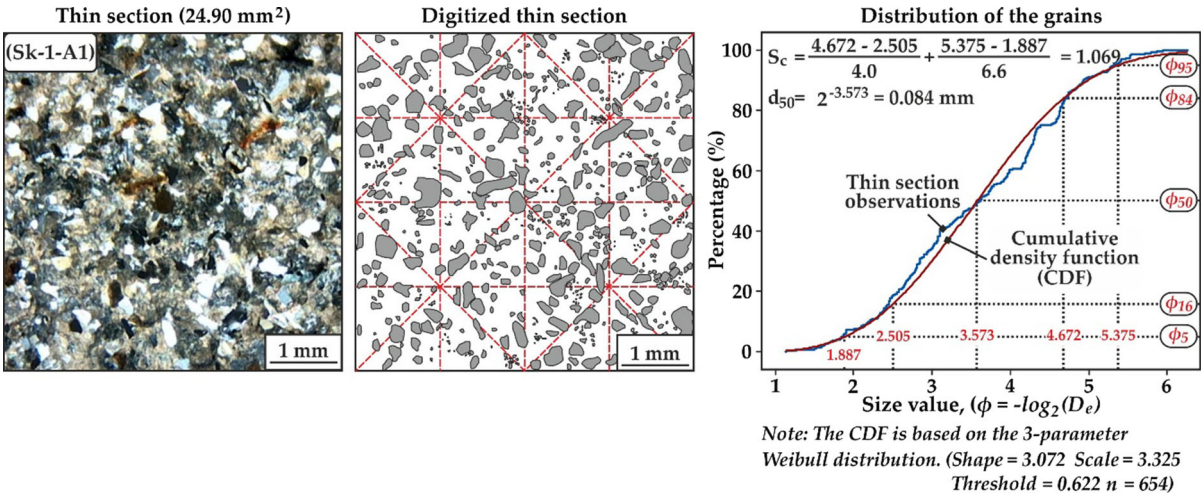

Figure 4. Determination of the d_{50} (mm) and S_c from thin-section analyses.

Table 1. Technical properties of the laboratory-scale cone crusher used in the study

Property	Value
Nominal voltage, V_n (V)	380
Nominal power, P_n (kW)	3.0
Rated current, I (A)	6.1
Frequency (Hz)	50
Feeding gape (mm)	≤ 30
Maximum feed size (mm)	≤ 25
Feeding capacity (kg/h)	≤ 100
Eccentric speed, E_s (rpm)	690–700
Power factor, cos(ϕ)	0.90
Efficiency (%)	86

Table 2. Apertures of bar sieves eligible for different particle sizes (BS-EN 933-3)

Particle size (mm)	Aperture of the bar sieve (mm)
12.5–16.0	8.00
10.0–12.5	6.30
8.0–10.0	5.00
6.3–8.0	4.00
5.0–6.3	3.15

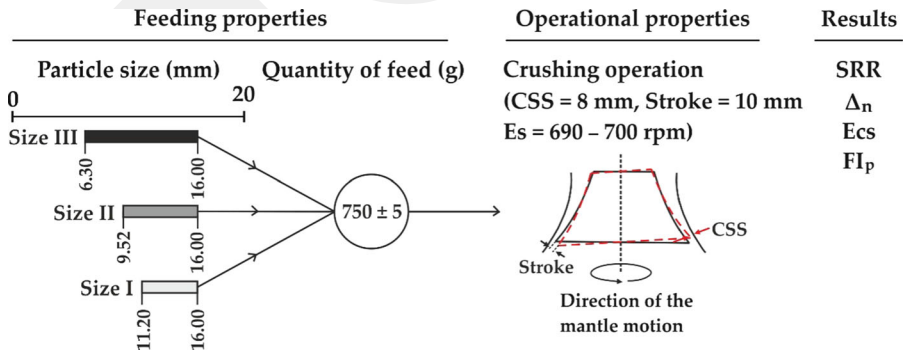

Figure 5. Experimental flowchart for the crushability tests.

More specifically, the apertures of bar sieves for flakiness index tests are given in Table 2. In case of particle sizes not conforming to Table 2, the closest size groups (e.g., for size II (+ 9.52 − 16.00 mm), an 8-mm bar sieve was used in a sub-fraction of + 12.50 − 16.00 mm and a 6.30-m bar sieve was used in a sub-fraction of − 12.50 mm + 9.52 mm) were adopted. In such cases, interpolations in conjunction with averages of sub-fraction feed and product masses were considered for the determination of flakiness index. In light of these explanations, flakiness indices of the feed (FI_f) and product (FI_p) were determined using the following equation:

$$FI_{f-p} = 100 \times \left(\frac{\sum_{i=1}^{n} m_2}{m_1} \right) \quad (10)$$

where m_2 is the total mass (g) of particles passing through the bar sieve/sieves in case of sub-fractions, n is the number of sub-fractions available (Table 2), and m_1 is the initial mass (g) of the particles tested.

LABORATORY STUDIES

Mineralogical, Textural, and Chemical Characterizations

Typical thin sections, SEM images of the crushed particles, mineralogical and textural features of the sandstones are listed in Table 3. Based on the thin-section analyses, the quartz (Qtz) content varied from 16 to 55%, whereas the feldspar (F) content including both plagioclase and alkali feldspar was between 6 and 35%. Lithic fragments (Lf) were observed as four different subgroups. They were gravel substitutions (e.g., micro-quartzite with undulose extinction (H-Qtz) and volcano-sedimentary particles), detritic igneous constituents (e.g., hornblende, biotite, tremolite, chlorite, and pyroxene), carbonate-based fragments (e.g., calcite, aragonite), and opaque minerals (e.g., magnetite, rutile). These subgroups as a whole were included in the Lf content, which varied from 38 to 65%.

From the mineralogical point of view, most of the sandstones had no weathering signs. In contrast, some of them (e.g., Sk–2, Sg–3, and Ska–7) presented chloritization, argillization, and opacitization. Chloritization was typical in biotites and hornblendes, whereas the argillization was apparent in feldspars. Opacitization was observed in the Lf contents, especially in pyroxenes, and other igneous detritics of the sandstones mentioned herein.

As for the textural features of the sandstones, the d_{50} was found to be between 0.114 and 0.596 mm, whereas the S_c ranged from 0.924 to 1.653. It was determined that higher values of S_c point out a higher degree of heterogeneity in the rock that has similarities with the d_{50}. The cement type of the sandstones was composed of a mixture of silica–clay particles lower than 20 μm.

From the SEM images of the crushed particles, one could notice that the crushing patterns of sandstones are quite different. Based on the data provided in Table 3, the sandstones were classified regarding their lithofacies and degree of sorting. According to Folk (1981), the investigated sandstones were identified from feldspathic litharenite to litharenite (Fig. 6a). Considering the sorting classification of Folk and Ward (1957), the sandstones were poorly sorted in most cases (Fig. 6b).

Physico-mechanical Properties

The physical and mechanical properties were determined using smooth-cut core samples with a diameter of 54.0 ± 0.2 mm under oven-dried conditions. The SH of rock materials was determined, using a C-2-type Shore scleroscope. The SH tests were carried out on rock surfaces (i.e., top and bottom surfaces) of core samples whose volume is greater than 80 cm^3. In total, 20 measurements were recorded for each rock surface. After this, the average value of the measurements was considered as the SH of rocks. The UCS of the sandstones was determined, using core samples with a length-to-diameter ratio of 2.0–3.0 (Fig. 7a). For the Brazilian tensile strength (BTS, MPa) tests, core samples with a height-to-diameter ratio of 0.5–1.0 were used (Fig. 7b). The UCS and BTS tests were repeated five times, and average values were reported. The physico-mechanical properties of the sandstones are listed in Table 4. Considering the UCS values in Table 4, the investigated sandstones were identified from moderately hard rock (UCS 50–100 MPa) to weak rock (UCS 25–50 MPa), according to Deere and Miller (1966).

Crushability Tests

Crushability tests provide quantitative data on sizing, production yield, and comminution rate of rock aggregates occurring in a laboratory–scale cone crusher (Fig. 7c).

Table 3. Mineralogical and textural features of the sandstones

Rock type	Thin section	SEM images of crushed particles passing through the 0.106-mm sieve	Mineralogical and textural features
Sk–1	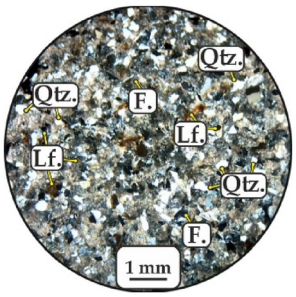	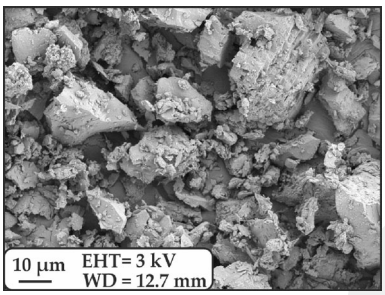	Quartz (Qtz) = 34% Feldspar (F) = 9% Lithic fragment (Lf) = 57% Cement type = Silica − clay Average grain size (d_{50}) = 0.114 mm Sorting coefficient (S_c) = 0.924 (Moderately sorted)
Sk–2	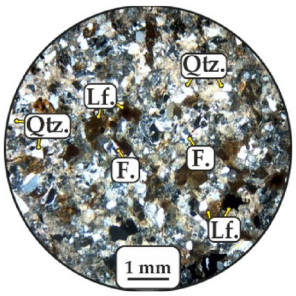	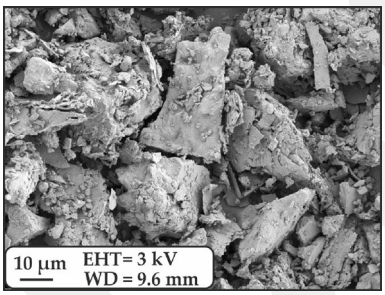	Quartz (Qtz) = 30% Feldspar (F) = 7% Lithic fragment (Lf) = 63% Cement type = Silica − clay Average grain size (d_{50}) = 0.211 mm Sorting coefficient (S_c) = 1.204 (Poorly sorted)
Sg–3	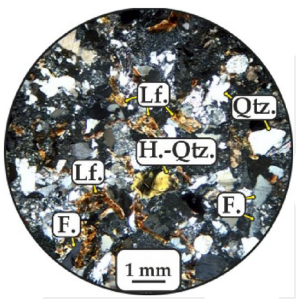	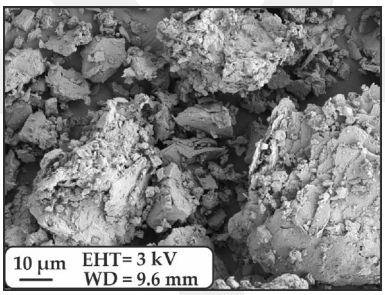	Quartz (Qtz) = 33% Feldspar (F) = 15% Lithic fragment (Lf) = 52% Cement type = Silica − clay Average grain size (d_{50}) = 0.344 mm Sorting coefficient (S_c) = 1.465 (Poorly sorted)
Sg–4	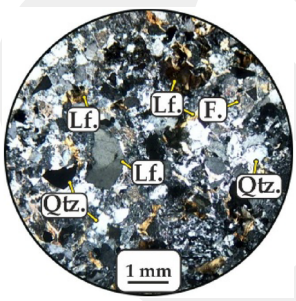	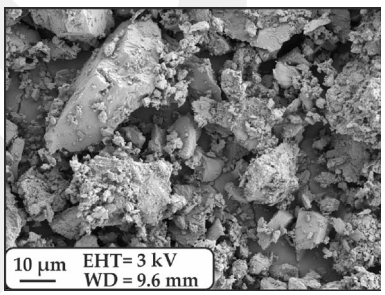	Quartz (Qtz) = 42% Feldspar (F) = 14% Lithic fragment (Lf) = 44% Cement type = Silica − clay Average grain size (d_{50}) = 0.283 mm Sorting coefficient (S_c) = 1.308 (Poorly sorted)

Table 3. continued

Rock type	Thin section	SEM images of crushed particles passing through the 0.106-mm sieve	Mineralogical and textural features
Sa–5	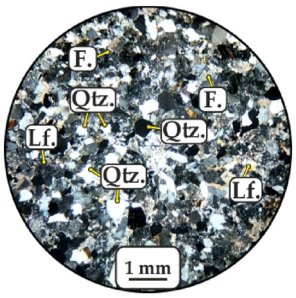	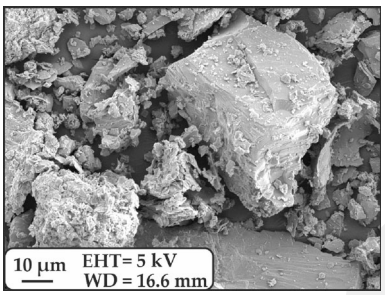	Quartz (Qtz) = 55% Feldspar (F) = 6% Lithic fragment (Lf) = 39% Cement type = Silica − clay Average grain size (d_{50}) = 0.229 mm Sorting coefficient (S_c) = 1.085 (Poorly sorted)
Sa–6	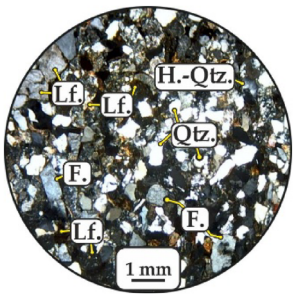	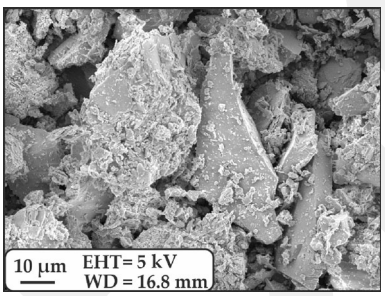	Quartz (Qtz) = 46% Feldspar (F) = 16% Lithic fragment (Lf) = 38% Cement type = Silica − clay Average grain size (d_{50}) = 0.332 mm Sorting coefficient (S_c) = 1.263 (Poorly sorted)
Ska–7	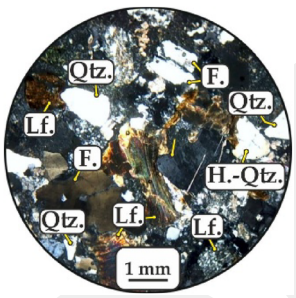	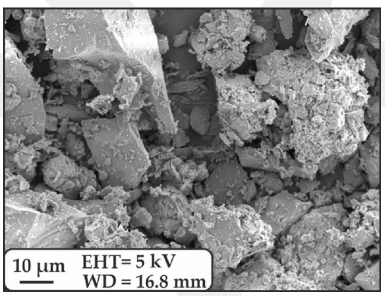	Quartz (Qtz) = 21% Feldspar (F) = 14% Lithic fragment (Lf) = 65% Cement type = Silica − clay Average grain size (d_{50}) = 0.596 mm Sorting coefficient (S_c) = 1.653 (Poorly sorted)
Saz–8	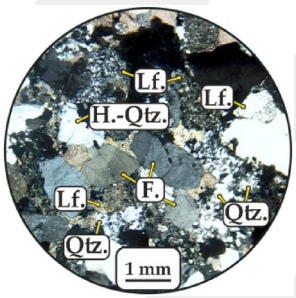	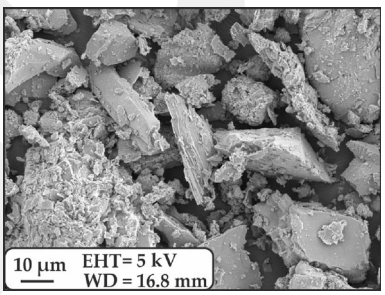	Quartz (Qtz) = 16% Feldspar (F) = 30% Lithic fragment (Lf) = 54% Cement type = Silica − clay Average grain size (d_{50}) = 0.476 Sorting coefficient (S_c) = 1.541 (Poorly sorted)

Table 3. continued

Rock type	Thin section	SEM images of crushed particles passing through the 0.106-mm sieve	Mineralogical and textural features
Saz–9	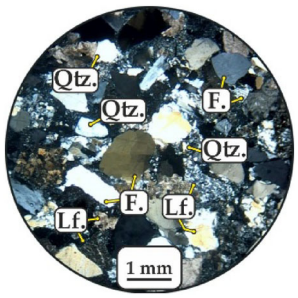	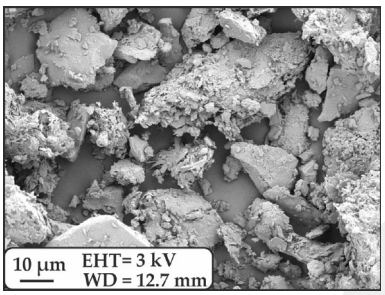	Quartz (Qtz) = 17% Feldspar (F) = 22% Lithic fragment (Lf) = 61% Cement type = Silica − clay Average grain size (d_{50}) = 0.420 mm Sorting coefficient (S_c) = 1.384 (Poorly sorted)
Sag–10	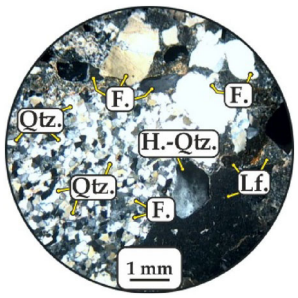	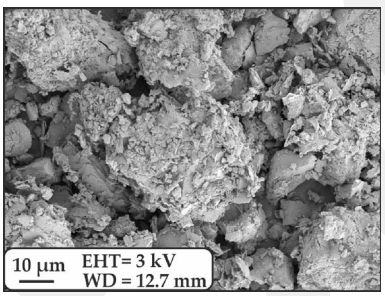	Quartz (Qtz) = 26% Feldspar (F) = 35% Lithic fragment (Lf) = 39% Cement type = Silica − clay Average grain size (d_{50}) = 0.289 mm Sorting coefficient (S_c) = 1.401 (Poorly sorted)

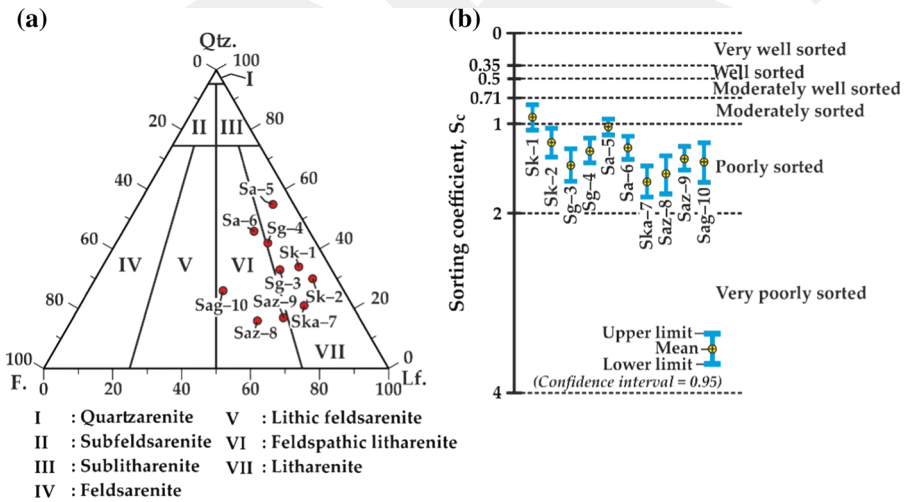

Figure 6. Mineralogical and textural characterizations of the sandstones: (**a**) Lithofacies classification of the sandstones based on Folk (1981). (**b**) Sorting classification of the sandstones based on Folk and Ward (1957).

Firstly, the size of relatively bigger sandstone blocks was reduced using a sledgehammer, and smaller blocks with a volume of 600–900 cm^3 were crushed by a Blake-type jaw crusher. By sieving the crushed rock blocks, rock aggregates with different size fractions (e.g., sizes I–III in Fig. 7e) were prepared for each rock type.

The number of flaky particles in the feeding material was also determined using Eq. (10) before crushability tests. Then, a total amount of 750 ± 5 g

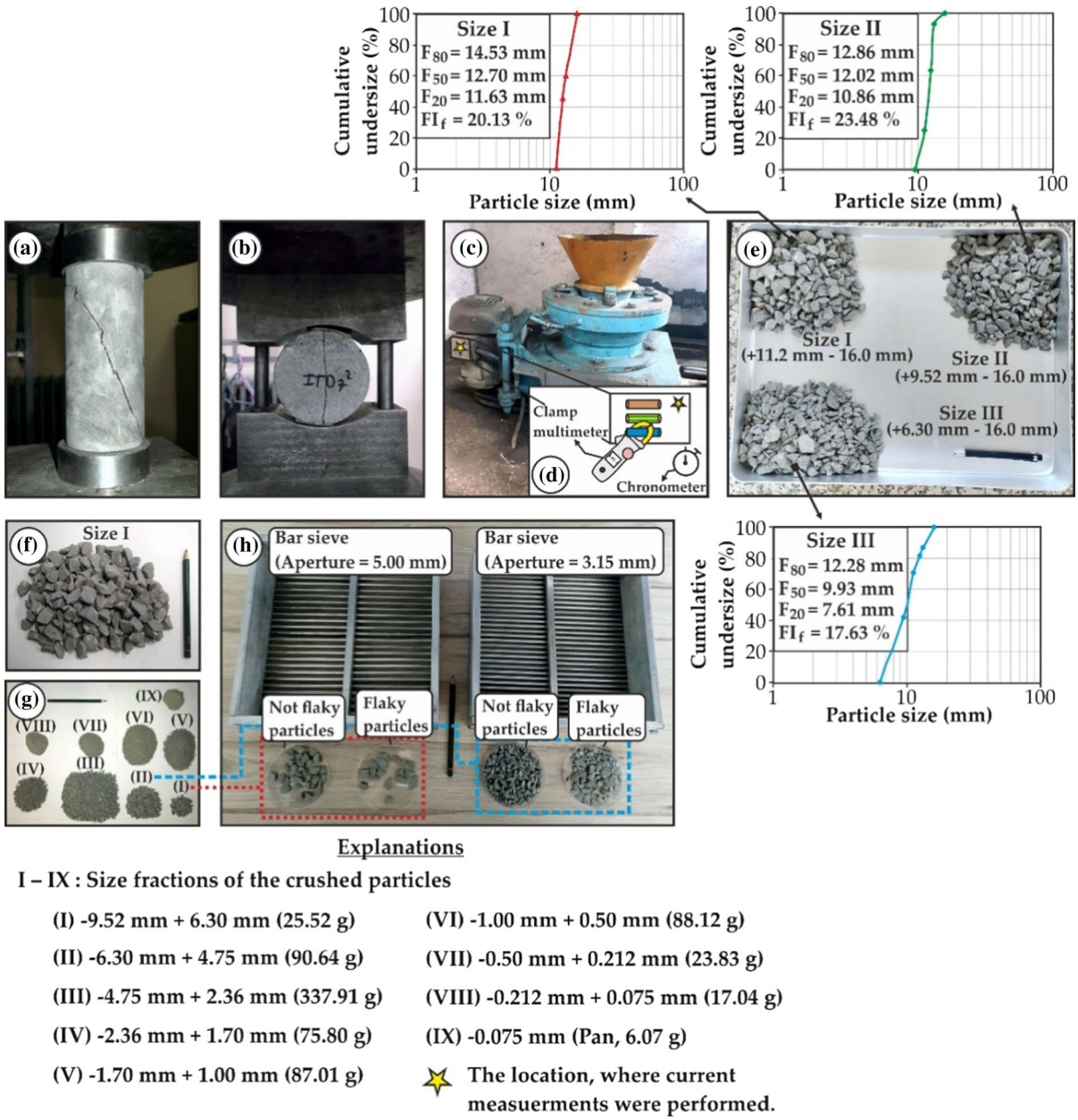

Figure 7. Laboratory equipment used and materials studied in physico-mechanical and crushability tests. (**a**) UCS test. (**b**) BTS test. (**c**) Laboratory-scale cone crusher used in crushability tests. (**d**) Schematic representation of current measurements drawn by the crusher. (**e**) Typical feeding materials with different size fractions. (**f**) A typical feeding material (size I) prepared before a crushability test. (**g**) Crushed particles of the product after a crushability test. (**h**) Flakiness index tests for crushed particles with different size fractions.

of rock aggregates was fed to the cone crusher, adopting the choke feeding method. The total amount of rock aggregates were fed to the cone crusher in a single charge by hand. During the crushability tests, the elapsed time ($T_{c,}$ s) and the current drawn ($I_{d,}$ A) by the crusher were recorded systematically. The T_c, and I_d were measured, utilizing a digital chronometer and a sensitive clamp multimeter, respectively (Fig. 7d). Before and after each crushability test, sieve analyses and flakiness

Table 4. Physical and mechanical properties of the sandstones

Rock type	ρ_d (g/cm^3)	n_e (%)	SH	UCS (MPa)	BTS (MPa)
Sk–1	2.60	2.03	59.82	83.31	8.59
Sk–2	2.58	3.39	51.44	72.04	5.34
Sg–3	2.47	5.69	57.06	41.63	2.14
Sg–4	2.62	5.13	57.94	74.83	5.84
Sa–5	2.57	1.27	68.92	93.13	9.50
Sa–6	2.62	0.78	62.85	54.22	7.12
Ska–7	2.51	7.39	40.60	32.85	1.75
Saz–8	2.51	6.51	43.08	53.77	3.61
Saz–9	2.50	5.73	49.41	62.11	3.39
Sag–10	2.49	4.21	45.85	57.03	4.26

ρ_d, dry density; n_e, apparent porosity; SH, shore hardness; UCS, uniaxial compressive strength; BTS, Brazilian tensile strength

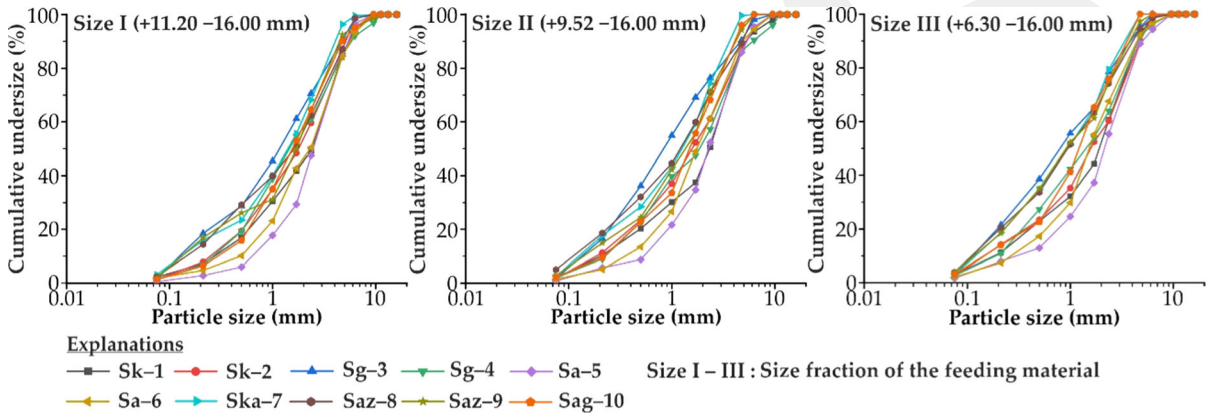

Figure 8. Typical PSDs of the products.

index tests were performed for feeding materials and final products (Fig. 7e–h). Because particles lower than 4 mm are not suitable for flakiness index tests (BS EN 933–3 2012), the FI_p was determined (Eq. 10) considering only two different size fractions, namely − 9.52 + 6.3 mm and − 6.3 mm + 4.75 mm. For these size fractions, 5.00-mm and 3.15-mm bar sieves were used, respectively (Fig. 7h).

The DRC of the sandstones was quantified, considering the variations in the SRR and Δ_n values that were determined by Eqs. (8) and (9), respectively. Typical PSDs of the products with different size fractions are shown in Figure 8. Based on these PSDs, the crushability test results are given in Table 5. The SRR of the sandstones varied from 3.15 to 5.05. The Δ_n and E_{cs} were found to be between 1.31 and 3.05 and 42.13 and 71.47 kJ/kg, respectively. The results in Table 5 show that the DRCs of the sandstones are quite different from one another. The underlying reasons for the varying DRCs are discussed below.

RESULTS AND DISCUSSION

Production Yield, Size, and Shape Properties

The crushability test results showed that the behavior of sandstones under compressive loading is quite different owing to the feeding size fractions and rock properties. As a result of these differences, different production yields were obtained for different size fractions. Figure 9 shows the variability of production yields for different size fractions (PY–1; PY–4). When combining the findings in Figure 9 with the mineralogical, textural, and physico-mechanical properties (Table 3, 4), it was statistically determined that the production yield for the size fractions of + 2.36 − 4.75 mm (PY–2) and − 1.00 mm (PY–4) has a close relationship with the BTS of rocks (Fig. 10).

The trends in the S_c also seemed to affect the production yields (Fig. 10). Since there was a close relationship between the S_c and d_{50} (i.e., $S_c = 1.39 + d_{50} + 0.86$, $R^2 = 0.79$), similar trends

Table 5. Crushability test results

Rock type	Size fraction	m_f (g)	FI_f %)	F_{80} (mm)	F_{50} (mm)	F_{20} (mm)	P_{80} (mm)	P_{50} (mm)	P_{20} (mm)	SRR	Δ_n	T_c (s)	E_T (kJ)	E_{cs} (kJ/kg)
Sk–1	Size I	750	20.13	14.53	12.70	11.63	4.26	2.41	0.58	3.41	1.53	26.8	47.14	65.47
	Size II	752	23.48	12.86	12.02	10.86	3.99	2.26	0.48	3.22	1.55	26.0	46.34	61.62
	Size III	749	17.63	12.28	9.93	7.61	3.54	1.89	0.41	3.47	1.66	26.2	46.56	62.16
Sk–2	Size I	751	16.33	14.28	12.36	11.72	4.03	1.77	0.51	3.54	1.99	25.1	45.78	60.96
	Size II	753	17.61	13.06	12.51	11.06	3.91	1.54	0.37	3.34	2.30	24.7	44.57	59.19
	Size III	750	18.65	11.84	9.85	7.58	3.62	1.56	0.38	3.27	2.08	24.2	45.25	60.34
Sg–3	Size I	751	17.69	14.59	12.66	11.88	3.28	1.14	0.23	4.45	2.68	19.2	34.22	45.57
	Size II	749	20.96	12.91	11.05	10.35	2.76	0.82	0.26	4.68	3.05	20.3	36.17	48.29
	Size III	752	19.34	12.09	9.70	7.54	2.44	0.78	0.19	4.95	2.88	20.5	37.20	49.47
Sg–4	Size I	751	15.80	14.46	12.54	11.59	4.04	1.44	0.51	3.58	2.45	23.1	38.18	50.84
	Size II	752	18.35	12.66	11.57	9.99	3.99	1.81	0.42	3.17	1.97	21.8	39.85	52.99
	Size III	749	16.64	11.95	10.10	7.40	3.47	1.39	0.34	3.44	2.25	22.5	40.07	53.50
Sa–5	Size I	750	20.47	14.20	12.28	11.50	4.31	2.41	1.08	3.29	1.34	28.8	53.42	71.23
	Size II	748	25.05	12.96	11.32	10.24	4.11	2.29	0.88	3.15	1.41	28.4	51.39	68.70
	Size III	750	17.61	12.14	10.08	7.46	3.86	2.10	1.10	3.15	1.31	29.2	53.60	71.47
Sa–6	Size I	750	15.28	14.16	12.35	11.58	4.26	2.25	0.81	3.32	1.53	26.1	47.39	63.19
	Size II	750	18.22	13.11	10.78	10.17	3.70	1.75	0.68	3.54	1.73	25.9	48.09	64.12
	Size III	753	15.66	12.30	10.18	7.22	3.28	1.50	0.56	3.75	1.81	26.3	49.66	65.95
Ska–7	Size I	752	16.90	14.37	12.63	11.47	3.14	1.44	0.33	4.58	1.95	18.9	31.68	42.13
	Size II	751	19.36	13.17	11.69	10.53	2.71	1.23	0.26	4.86	1.99	20.4	33.15	44.14
	Size III	750	18.01	12.23	10.06	7.10	2.42	0.91	0.24	5.05	2.40	20.8	32.51	43.35
Saz–8	Size I	748	23.12	14.39	12.14	11.38	3.74	1.64	0.30	3.85	2.10	21.6	38.11	50.95
	Size II	750	18.50	12.68	11.54	10.38	3.28	1.18	0.23	3.87	2.58	22.2	39.60	52.80
	Size III	751	16.74	12.14	9.70	7.26	2.79	0.91	0.21	4.41	2.84	21.9	39.82	53.02
Saz–9	Size I	750	17.50	14.11	12.39	11.30	3.39	1.70	0.28	4.16	1.83	19.7	34.93	46.59
	Size II	752	16.66	12.80	12.02	10.45	2.99	1.36	0.33	4.28	1.96	18.5	33.12	44.04
	Size III	749	18.26	12.04	9.62	7.05	2.71	0.88	0.23	4.44	2.82	19.3	35.28	47.10
Sag–10	Size I	748	18.16	14.37	12.57	11.86	3.57	1.54	0.55	4.03	1.96	20.3	36.55	48.86
	Size II	751	17.49	12.53	11.39	10.94	3.11	1.45	0.40	4.03	1.87	20.6	36.74	48.92
	Size III	750	14.95	11.56	9.61	7.14	2.64	1.19	0.38	4.38	1.90	20.2	36.13	48.17

Size I: + 11.20 mm − 16.00 mm, Size II: + 9.52 mm − 16.00 mm, Size III: + 6.30 − 16.00 mm

were also obtained for varying d_{50} values. In general, the increase in the S_c poses heterogeneity in the rock, and therefore, fine crushing resistance of the sandstones is associated with the rock texture. On the other hand, although the mineralogical variable of Qtz content could be correlated with the BTS and SH of the sandstones ($BTS = 0.16Qtz + 0.09$, $R^2 = 0.56$, $SH = 0.65Qtz + 32.52$, $R^2 = 0.80$), the mineralogical features (i.e., Qtz, F, and Lf contents) do not affect size reduction.

From size I to size III type of feeding, the intensity of choke feeding increased by generating relatively higher release surfaces in/around the mineral grains. This case probably intensified the shear forces among grains during the crushing action. Consequently, the number of fine particles (PY–4) increased with the intensity of choke feeding that conforms to the findings of Guimaraes et al. (2007). The production yields could also be assessed, focusing on the variations in the Δ_n. In other words, increasing the Δ_n could give a relative measure in higher product achievements for the PY–4 but lower for the PY–2 (Fig. 11).

The degree of product flakiness is dependent upon the composition of the material fed to the cone crusher (Bengtsson and Evertsson 2006). It can be said that the variations in feeding type (size I–size III), irrespective of whether mineralogical, textural, or physico-mechanical properties, influence the FI_p. In this direction, the findings in Figure 12 support the conclusions of Eloranta (1995) and Bengtsson and Evertsson (2006).

The change in feeding size (size I–size III) controls the intensity of choke feeding. Therefore, it has a close relationship with the product flakiness and PSD of products (Figs. 8, 9, 10, 11, and 12). Furthermore, based on the statistical analyses, there was no significant evidence indicating that the FI_f acts on the FI_p.

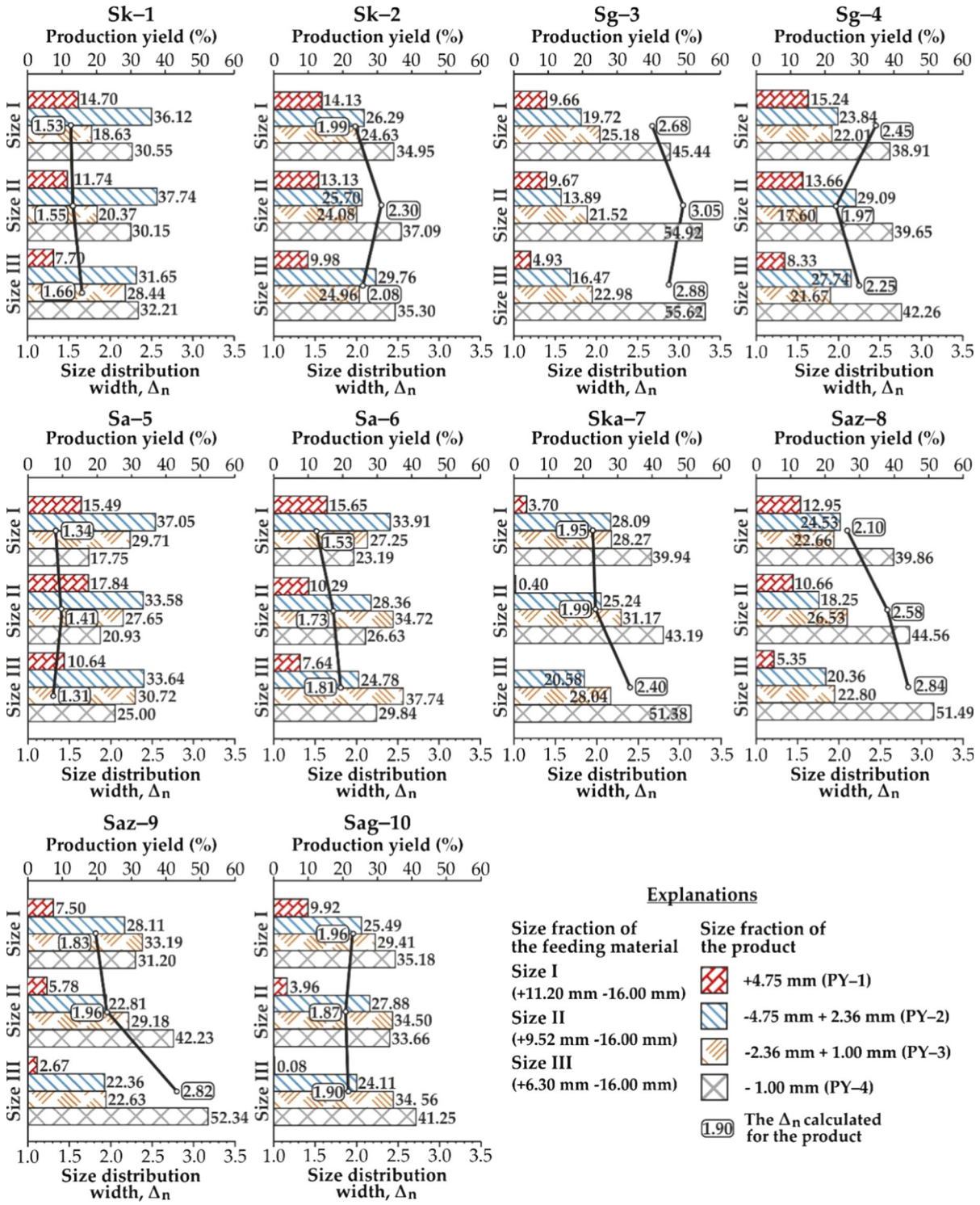

Figure 9. Production yields after crushability tests.

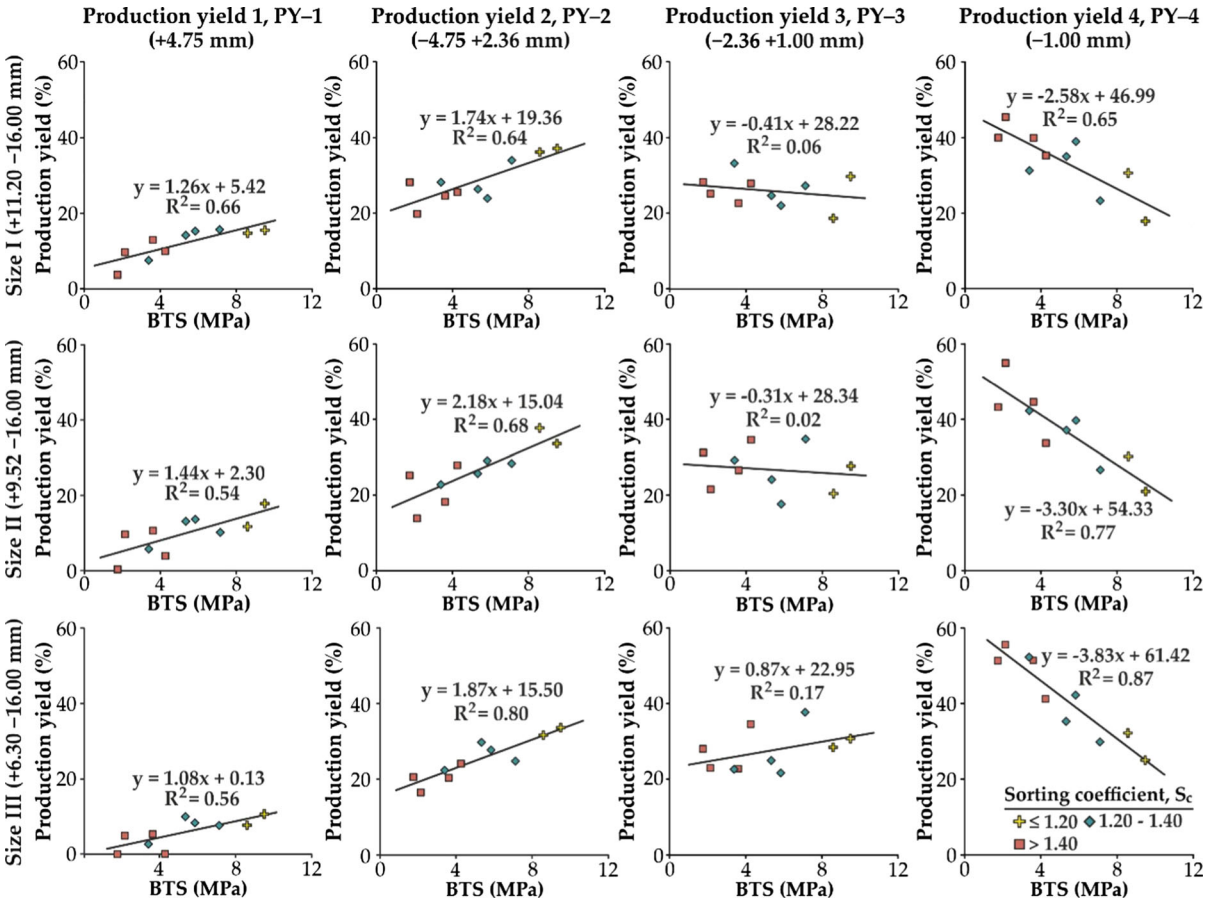

Figure 10. Variations in the production yield arising from varying BTS of the sandstones.

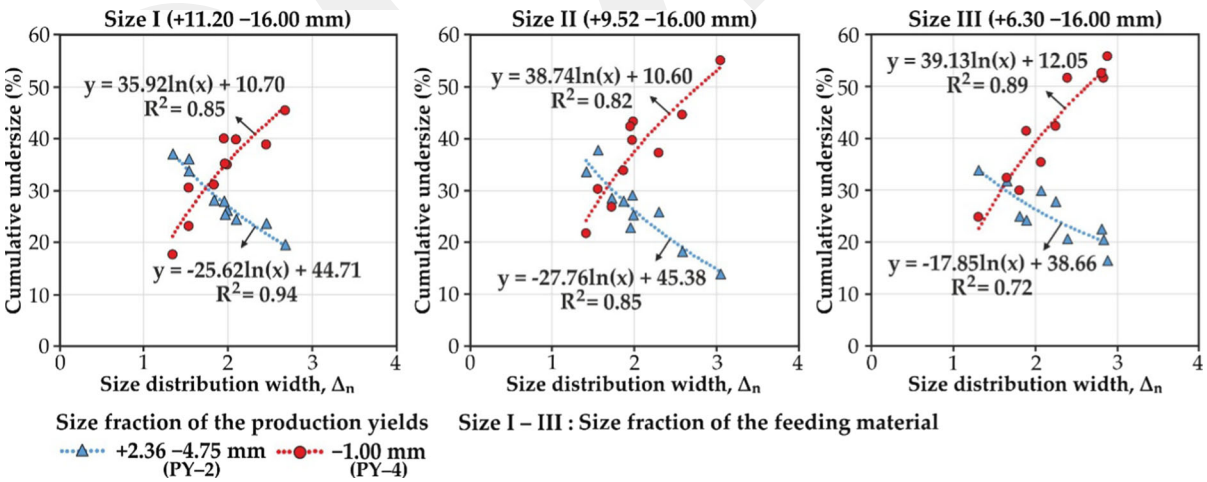

Figure 11. Relationships between the Δ_n and the production yields of different size fractions.

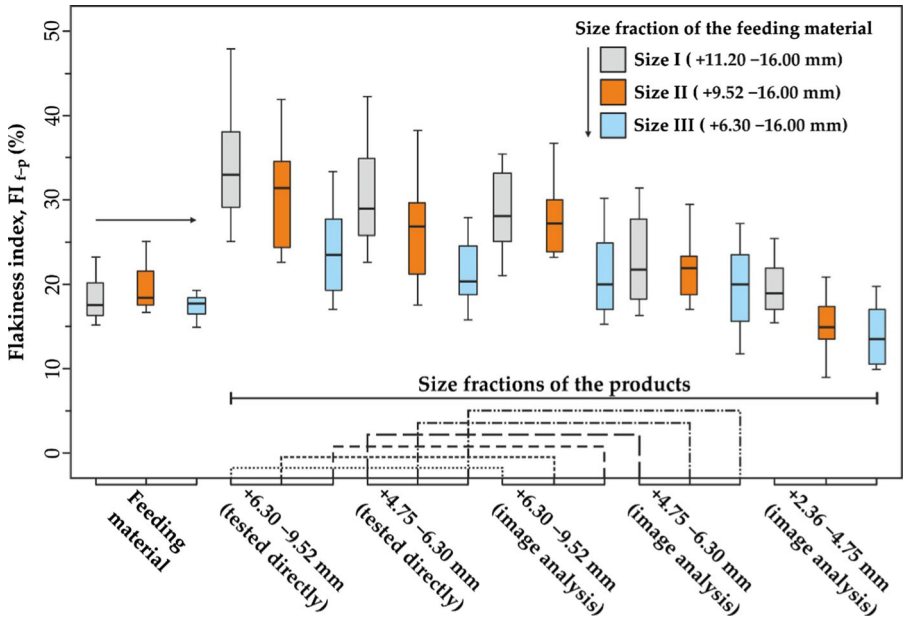

Figure 12. Flakiness indices of the materials.

Nevertheless, the probable effects of FI_f on the FI_p should be further investigated since they were not considered in this study.

Depending on the flakiness degree of feeding materials and products, the FI_f was found to be between 16 and 18% on average. For all rock types, the average FI_p decreased slightly by decreasing the size fractions ranging from + 6.30 − 9.52 mm to + 4.75 − 6.30 mm (Fig. 12). The decrease in the FI_p for these size fractions was also supported by the image analysis results. However, the image analyses provided lesser FI_p values compared to those obtained from the flakiness index tests. Moreover, the FI_p continued to decrease with the size fraction of + 2.36 − 4.75 mm.

In addition to shape-based evaluations, the investigated sandstones as a tailing material could be evaluated in different applications. Porous sandstones, as a potential source of rock aggregates, were reported as a non-suitable material for paving mixtures (Gayana and Ram Chandar 2018). Nevertheless, several studies also reported that various sandstones could be feasible for concrete structures by using them directly or replacing them with other aggregate sources (Kumar 2006; Kumar et al. 2016; Ram Chandar et al. 2016). Notably, non-friable and low porous sandstones could be considered for concrete aggregates (Alexander and Mindess 2005). Besides, Kotarska et al. (2018) emphasized sandstones eligible for the production of autoclaved aerated concrete (AAC).

Based on the previous studies mentioned herein, some of the investigated sandstones (i.e., Sg–3, Sg–4, Ska–7, Saz–8, Saz–9) were found to be moderate-porous rocks ($n_e \geq 5\%$), according to Anon (1979). Therefore, their potential use or performance in paving or concrete mixtures could not be suitable. However, the ones with relatively lower porosity and higher strength properties (e.g., Sk–1, Sa–5, Sa–6) could be further investigated for their use as fine aggregate or subbase material. Moreover, the investigated sandstones could be further investigated with regards to raw materials aiming at the AAC production owing to their increasing tonnage in the ZHB.

From size I to size III type of feeding, the effect of BTS was more visible on the product achievements of the PY–2 and PY–4 when the correlations of determination (R^2) in Figure 10 are considered. The products retained on the 4.75-mm sieve (PY–1) were less correlative with the BTS of rocks. Moreover, no statistically meaningful relationship was obtained between the products of + 1.00 − 2.36 mm (PY–3) and the BTS of rocks.

To reveal the actual suitability of the sandstones for use in different applications, other

Table 6. Remarkable relationships obtained in this study

Independent variable	Empirical formula	Estimate	Std. error.	*t* value	*F* value	R^2
BTS	$E_{cs(av)} = 38.17 + 3.23\text{BTS}$	38.17	2.56	14.91	52.22	0.85
		3.23	0.45	7.18		
n_e	$E_{cs(av)} = 70.24 - 3.66n_e$	70.24	2.75	25.54	39.74	0.81
		− 3.66	0.58	− 6.31		
S_c	$E_{cs(av)} = 100.80 - 34.76S_c$	100.80	11.21	8.99	17.22	0.64
		− 34.76	8.38	− 4.15		
BTS	$\text{SRR}_{(av)} = 4.95 - 0.20\text{BTS}$	4.95	0.19	26.05	38.39	0.83
		− 0.20	0.03	− 6.67		
S_c	$\text{SRR}_{(av)} = 0.86 + 2.29S_c$	0.86	0.70	1.22	18.87	0.67
		2.29	0.53	4.32		
BTS	$\Delta_{n(av)} = 2.79 - 0.14\text{BTS}$	2.79	0.19	14.68	17.56	0.65
		− 0.14	0.03	4.67		
n_e	$\Delta_{n(av)} = 1.42 + 0.15n_e$	1.42	0.21	6.76	12.12	0.55
		0.15	0.04	3.75		

BTS, Brazilian tensile strength; n_e, apparent porosity, S_c, sorting coefficient

Table 7. Descriptive statistics of the crushing operations in this study

Value	F_{80} (mm)	P_{80} (mm)	BTS (MPa)	E_{cs} (kJ/kg)
Min.	11.56	2.42	1.75	71.47
Max.	14.59	4.31	9.50	42.13
Mean	13.09	3.44	5.15	54.84
SD	0.98	0.57	2.53	8.88
Cov. (%)	7.48	16.57	49.12	16.19
n	30	30	30	30

Operational factors: CSS = 8 mm, stroke = 10 mm, E_s = 690–700 rpm, *Min.* minimum value, *Max.* maximum value, *SD* standard deviation, *Cov* coefficient of variation, *n* number of observations

aggregate tests such as Los Angeles abrasion (LAA, %) and magnesium sulfate soundness (M_{wl}, %) should also be performed. In any case, the crushability test results provide a piece of knowledge about the degradation potential or crushing/fragmentation resistance of rocks, some of which are shown in Figures 9, 10 and 11.

In parallel with this statement, the crushability tests could also be considered to estimate the LAA of rocks (Kahraman and Toraman 2008; Teymen 2019).

Size Reduction Assessment

The crushability test results showed that the SRR increases gradually from the size I to size III type of feeding for the sandstones whose BTS is relatively low (e.g., Sg–3, Ska–7). However, for the sandstones with higher BTS (e.g., Sk–1, Sg–4, and Sa–5), the variations in the SRR are changeable, which could be attributed to brittle failure during the crushing actions in cone crusher.

Statistically meaningful relationships are listed in Table 6. Based on the average SRR, E_{cs}, and Δ_n values of the three different feeding sizes (e.g., $\text{SRR}_{(av)}$, $E_{cs(av)}$), the energy consumption and relative success of crushing operations are associated with the BTS, n_e, and S_c of the sandstones (Table 6). Moreover, the production yield profile, which was quantified as the Δ_n, could be correlated with the BTS and n_e. However, the variations in feeding size fractions are more effective on the Δ_n (Fig. 11). The crushability test results were also utilized to achieve a theoretical base on the sandstone crushability in the cone crusher. Based on the crushing operational factors (Fig. 4), the variations in the BTS were integrated into the crushability test results. In this way, a new data set available to regression analysis was constructed (Table 7).

By employing additional regression analyses, the energy consumption during crushing actions in the cone crusher was put forward as a size-related empirical formula (Eq. 11). Although the correlation of determination ($R^2 = 0.64$) for Eq. (11) was not high enough, it could have given a theoretical knowledge on the sandstone breakage characteristics for cone crushers.

$$E_{cs} = 39.19\text{BTS}\left[\frac{1}{\sqrt{P_{80}}} - \frac{1}{\sqrt{F_{80}}}\right],\ R^2 = 0.64. \quad (11)$$

With several modifications, Eq. (11) resembles the Bond's work index (Bond 1961), easy to understand, and shows the variability of product size, rock

strength, and specific energy consumption in cone crusher. However, it should be kept in mind that Eq. (11) is only valid under the framework of the crushing operations, and methodologies followed in this study (Fig. 4, Table 7).

Thus, the empirical formula should be improved by further crushability tests, using a significant number of sandstones with different textural features, adopting various feeding size fractions, and operational factors such as the CSS and Es adjustments in cone crusher. In this way, comprehensive inferences could be achieved for sandstone crushability in cone crushers.

CONCLUSIONS

The present study aims to reveal the size reduction characterization of several underground mine tailings in the ZHB. These tailings are mainly sandstones with different mineralogical and textural features. The size reduction characterization of the sandstones is based on several crushability tests. The laboratory test results indicated that the DRC and E_{cs} are dependent upon the BTS and n_e of the sandstones. The S_c also influences the E_{cs}. The other results obtained from the present study could be drawn as follows:

- Mineralogical features of the sandstones have no significant effect on the size reduction processes, but the textural features do to some extent. Notably, the S_c (Eq. 5) could be considered for further studies about sandstone crushability in cone crusher. It might be claimed that the variations in the S_c could give a rapid estimation of the sandstone crushability when connected to their cementation/diagenesis degree.
- The intensity of choke feeding increases from size I to III type of feeding in the crushing actions. This phenomenon leads to generating higher amounts of fines (Fig. 9). However, the increase in the intensity of choke feeding improves the product's flakiness at the same time (Fig. 12). Therefore, the variations in feeding size distributions should be considered for optimal or targeted product achievements in sandstone crushing that occurred in the cone crusher.
- The DRC could be quantified by considering the variations in the SRR and Δ_n (Table 5). The SRR provides knowledge on the success of crushing operations, whereas the Δ_n could be utilized for the assessment production yield rate. For a comprehensive assessment of sandstone crushability in cone crusher, these two variables should be considered together.
- Based on the BTS of sandstones, a simple empirical formula was derived (Eq. 11). It is a size-related empirical formula, easy to understand, and shows the importance of tensile strength as an indicator for sandstone crushability that occurred in cone crusher. However, the empirical formula should be improved by further crushability tests.

Undoubtedly, satisfactory results about crushability and grindability of sandstones through various crushers/mills could provide information/data about their potential use as construction and building materials. With a healthy integration of crushing and grinding processes, nearly 100% recovery could be achieved for these sandstone tailings located in the ZHB. The present study, on this point, could be declared a start-up, and further efforts are required to find and address possible usage areas for these sandstone tailings with all their derivatives from millimeter to the nanometer scale.

ACKNOWLEDGMENTS

The author is greatly indebted to Prof. Dr. Ahmet Özarslan, Dr. Mehmet Bilen, and technician Hasan Angın (Zonguldak Bulent Ecevit Univerisity, Turkey) for providing laboratory facilities and helping during laboratory studies. The author appreciates the invaluable help and efforts of technician Mehmet Güngör (Pamukkale University, Turkey) who prepared the thin sections, and research assistant Ahmet Faruk Yazıcı (Abdullah Gül University, Turkey) who helped at obtaining the SEM images. The author is also thankful to the Turkish Hard Coal Enterprise Institution (TTK, Zonguldak—Turkey) and anonymous mining companies who provided sandstone blocks and shared

their experiences. Last but not least, special thanks are due to the anonymous reviewers and handling editor for constructive comments and suggestions that improved the study.

REFERENCES

Akçaoğlu, T., Tokyay, M., & Çelik, T. (2004). Effect of coarse aggregate size and matrix quality on ITZ and failure behavior of concrete under uniaxial compression. *Cement and Concrete Composites, 26*(6), 633–638.

Alexander, M., & Mindess, S. (2005). *Aggregates in concrete*. Modern Concrete Technology Series 13, ISBN, 0-203-96369-5.

Anon, O. H. (1979). Classification of rocks and soils for engineering geological mapping, part 1—Rock and soil materials. *Bulletin of Engineering Geology and the Environment, 19*(1), 364–371.

Bearman, R. A., Briggs, C. A., & Kojovic, T. (1997). The application of rock mechanics parameters to the prediction of comminution behavior. *Minerals Engineering, 10*(3), 255–264.

Bengtsson, M., & Evertsson, C. M. (2006). An empirical model for predicting flakiness in cone crushing. *International Journal of Mineral Processing, 79*(1), 49–60.

Bengtsson, M., Hulthén, E., & Evertsson, C. M. (2015). Size and shape simulation in a tertiary crushing stage, a multi objective perspective. *Minerals Engineering, 77,* 72–77.

Bhaadani, K., Asbjörnsson, G., Hulthén, E., & Evertsson, M. (2020). Development and implementation of key performance indicators for aggregate production using dynamic simulation. *Minerals Engineering, 145,* 106065.

Bond, F. C. (1961). Crushing and grinding calculations Part II. *British Chemical Engineering, 6*(8), 543–548.

Briggs, C., & Evertsson, C. M. (1998). Shape potential of rock. *Minerals Engineering, 11*(2), 125–132.

BS EN 13450. (2002). British Standards Institution; Aggregates for railway ballast.

BS EN 933–3. (2012). British Standards Institution; Tests for geometrical properties of aggregates. Determination of particle shape. Flakiness index.

Chen, J. S., Chang, M. K., & Lin, K. Y. (2005). Influence of coarse aggregate shape on the strength of asphalt concrete mixtures. *Journal of the Eastern Asia Society for Transportation Studies, 6*(4), 1062–1075.

Chen, B., & Liu, J. (2007). Investigation of effects of aggregate size on the fracture behavior of high performance concrete by acoustic emission. *Construction and Building Materials, 21*(8), 1696–1701.

Coree, B. J., & Hislop, W. P. (2000). *A laboratory investigation into the effects of aggregate related factors of critical VMA in asphalt paving mixture*. Iowa DOT ProjectTR-415, CTRE Management Project 98-20, Center for Transportation Research and Education, Iowa State University.

Deere, D. U., & Miller, R. P. (1966). *Engineering classification and index properties for intact rock*. Technical Report Air Force Weapons Laboratory (Report No, AFWL-TR-65-116), 136–184, New Mexico.

Dickinson, W. R. (1970). Interpreting detrital modes of graywacke and arkose. *Journal of Sedimentary Petrology, 40*(2), 695–707.

Djordjevic, N., Shi, F. N., & Morrison, R. D. (2003). Applying discrete element modelling to vertical and horizontal shaft impact crushers. *Minerals Engineering, 16*(10), 983–991.

Donovan, J. G. (2003). *Fracture toughness based models for the prediction of power consumption, product size, and capacity of jaw crushers*. Dissertation, Virginia Polytechnic Institute, and State University.

Elices, M., & Rocco, C. G. (2008). Effect of aggregate size on the fracture and mechanical properties of a simple concrete. *Engineering Fracture Mechanics, 75*(13), 3839–3851.

Eloranta, J. (1995). *Influence of crushing process variables on the product quality of crushed rock*. Dissertation, Tampere University of Technology.

Evertsson, C. M. (1999). Modelling of flow in cone crushers. *Minerals Engineering, 12*(12), 1479–1499.

Folk, R. L. (1981). *Petrology of sedimentary rocks*. Austin: Hemphill Pub. ISBN: 0-914696-14-9.

Folk, R. L., & Ward, W. C. (1957). Brazos River bar, a study in the significance of grain size parameters. *Journal of Sedimentary Petrology, 27*(1), 3–26.

Gayana, B. C., & Ram, Chandar K. (2018). Sustainable use of mine waste and tailings with suitable admixture as aggregates in concrete pavements—A review. *Advances in Concrete Construction, 6*(3), 221–243.

Golalipour, A., Jamshidi, E., Niazi, Y., Afsharikia, Z., & Khadem, M. (2012). Effect of aggregate gradation on rutting of asphalt pavements. *Procedia-Social and Behavioral Sciences, 53,* 440–449.

Guimaraes, M. S., Valdes, J. R., Palomino, A. M., & Santamarina, J. C. (2007). Aggregate production, fines generation during rock crushing. *International Journal of Mineral Processing, 81*(4), 237–247.

Gupta, A., & Yan, D. (2016). *Mineral processing, design, and operations, an introduction* (2nd Ed.). Elsevier Press. ISBN: 978-0-444-63589-1.

Heikkilä, P. (1991). *Improving the quality of crushed rock aggregate*. Dissertation, Helsinki University of Technology.

Huebscher, R. G. (1948). Friction equivalents for round square and rectangular ducts. *ASHVE Transactions, 54,* 101–118.

ISRM. (2007). The complete ISRM suggested methods for rock characterization, testing, and monitoring, 1974–2006. In: R. Ulusay, & J. A. Hudson (Eds.), *Suggested methods prepared by the commission on testing methods*. International Society of Rock Mechanics (ISRM), Ankara, Turkey.

Itävuo, P., Vilkko, M., & Jaatinen. (2013). Indirect particle size distribution control in cone crushers. In *16th IFAC Symposium on automation in mining, mineral and metal processing* (pp. 224–229).

Kahraman, S., & Toraman, O. Y. (2008). Predicting Los Angeles abrasion loss of rock aggregates from crushability index. *Bulletin of Material Science, 31*(2), 173–177.

Khasawneh, M. A., & Alsheyab, M. A. (2020). Effect of nominal maximum aggregate size and aggregate gradation on the surface frictional properties of hot mix asphalt mixtures. *Construction and Building Materials, 244,* 118355.

Kim, S., Shen, J., & Jeong, M. M. (2018). Effects of aggregate size on the rutting and stripping resistance of recycled asphalt mixtures. *Journal of Materials in Civil Engineering, 30*(2), 04017280.

Köken, E., & Özarslan, A. (2018). New testing methodology for the quantification of rock crushability, compressive crushing value (CCV). *International Journal of Minerals, Metallurgy, and Materials, 25*(11), 1227–1236.

Korman, T., Bedekovic, G., Kujundzic, T., & Kuhinek, D. (2015). Impact of physical and mechanical properties of rocks on energy consumption of jaw crusher. https://doi.org/10.5277/ppmp150208.

Kotarska I., Mizera B., & Stefanek P. (2018). Mining waste in the circular economy–Idea versus reality. In *3rd Interntional Innovative Mining Symposium*. https://doi.org/10.1051/e3sconf/20184102013.

Kozul, R., & Darwin, D. (1997). *Effects of aggregate type, size and content on concrete strength and fracture energy*. Structural Engineering and Engineering Materials Report (No, 43), University of Kansas Center for Research Inc.

Kuity, A., & Das, A. (2016). Study on aggregate size distribution in asphalt mix using images obtained by different imaging techniques. *Transportation Research Proceedings, 17,* 340–348.

Kumar, S. (2006). *A study on high performance concrete using sandstone aggregates*. Dissertation, School of Engineering and Information Technology, Universiti Malasia Sabah.

Kumar, S., Gupta, R. C., & Shrivastava, S. (2016). Strength, abrasion and permeability studies on cement concrete containing quartz sandstone coarse aggregates. *Construction and Building Materials, 125,* 884–891.

Lee, E., & Evertsson, C. M. (2011). A comparative study between cone crushers and theoretically optimal crushing sequences. *Minerals Engineering, 24*(3–4), 188–194.

Leiva, C. A., Arcos, K. V., Poblete, D. A., Serey, E. A., Torres, C. M., & Ghorbani, Y. (2018). Design and evaluation of an expert system in a crushing plant. *Minerals, 8*(10), 469.

Lynch, A. (2015). *Comminution handbook–Spectrum 21*. The Australasian Institute of Mining and Metallurgy, ISBN, 978-1-925100-38-9.

Ma, Y., Fan, X., & He, Q. (2016). Prediction of cone crusher performance considering liner wear. *Applied Science, 6*(12), 404.

Major, K. (2002). Types and characteristics of crushing equipment and circuit flowsheets. In A. L. Mular, et al. (Eds.), *Mineral processing plant design, practice, and control* (pp. 566–583). Littleton, CO: SME.

Major, K. (2009). Factors influencing the selection and sizing of crushers. In D. Malhotra, et al. (Eds.), *Recent advances in mineral processing plant design* (pp. 356–360). Englewood: SME.

Metso. (2018). Basics in mineral processing handbook. Metso Corporation.

Mitchell, C. J., Mitchell, P., & Pascoe, R. D. (2008). Quarry fines minimisation, Can we really have 10 mm aggregate with no fines? In P. W. Scott, & G. Walton (Eds.), *Proceedings of the 14th extractive industry geology conference* (pp. 37–44).

Nikolov, S. (2004). Modelling and simulation of particle breakage in impact crushers. *International Journal of Mineral Processing, 74*(10), S219–S225.

Numbi, B. P., Xia, X., & Zhang, J. (2014). Optimal energy control modelling of a vertical shaft impact crushing process. *Energy Procedia, 61,* 560–563.

Rajan, B., & Singh, D. (2020). Investigation on effects of different crushing stages on morphology of coarse and fine aggregates. *International Journal of Pavement Engineering, 21*(2), 177–195. https://doi.org/10.1080/10298436.2018.1449951.

Ram Chandar, K., Gayana, B. C., & Sainath, V. (2016). Experimental investigation for partial replacement of fine aggregates in concrete with sandstone. *Advances in Concrete Construction, 4*(4), 243–261.

Sadrmomtazi, A., Lotfi-Omran, O., & Nikbin, I. M. (2020). Influence of cement content and maximum aggregate size on the fracture parameters of magnetite concrete using WFM, SEM, and BEM. *Theoretical and Applied Fracture Mechanics, 107,* 102482. https://doi.org/10.1016/j.tafmec.2020.102482.

Smith, M. R., & Collis, L. (2001). *Aggregates sand, gravel and crushed rock aggregate for construction purposes* (3rd ed., p. 360). London: Geological Society of London.

Teymen, A. (2019). Estimation of Los Angeles abrasion resistance of igneous rocks from mechanical aggregate properties. *Bulletin of Engineering Geology and the Environment, 78,* 837–846.

Ulsen, C., Tseng, E., Angulo, S. C., Landmann, M., Contessotto, R., Balbo, J. T., et al. (2019). Concrete aggregate properties crushed by jaw and impact secondary crushing. *Journal of Materials Research and Technology, 8*(1), 494–502.

Vu, X. H., Daudville, L., & Malecot, Y. (2011). Effect of coarse aggregate size and cement paste volume on concrete behavior under high triaxial compression loading. *Construction and Building Materials, 25*(10), 3941–3949.

Wills, B. A., & Finch, J. A. (2015). *Wills' mineral processing technology, an introduction to the practical aspects of ore treatment and mineral recovery*. London: Butterworth-Heinemann.